ICES REPORT 11-25

July 2011

Generalization of the Twist-Kirchhoff Theory of Plate Elements to Arbitrary Quadrilaterals and Assessment of Convergence

by

H.A.F.A Santos, J.A. Evans, and T.J.R. Hughes

The Institute for Computational Engineering and Sciences
The University of Texas at Austin
Austin, Texas 78712

Reference: H.A.F.A Santos, J.A. Evans, and T.J.R. Hughes, "Generalization of the Twist-Kirchhoff Theory of Plate Elements to Arbitrary Quadrilaterals and Assessment of Convergence", ICES REPORT 11-25, The Institute for Computational Engineering and Sciences, The University of Texas at Austin, July 2011.

Report Documentation Page

Form Approved
OMB No. 0704-0188

1. REPORT DATE **JUL 2011**	2. REPORT TYPE	3. DATES COVERED **00-00-2011 to 00-00-2011**

4. TITLE AND SUBTITLE **Generalization of the Twist-Kirchhoff Theory of Plate Elements to Arbitrary Quadrilaterals and Assessment of Convergence**	5a. CONTRACT NUMBER 5b. GRANT NUMBER 5c. PROGRAM ELEMENT NUMBER
6. AUTHOR(S)	5d. PROJECT NUMBER 5e. TASK NUMBER 5f. WORK UNIT NUMBER
7. PERFORMING ORGANIZATION NAME(S) AND ADDRESS(ES) **University of Texas at Austin,Institute for Computational Engineering and Sciences,Austin,TX,78712**	8. PERFORMING ORGANIZATION REPORT NUMBER
9. SPONSORING/MONITORING AGENCY NAME(S) AND ADDRESS(ES)	10. SPONSOR/MONITOR'S ACRONYM(S) 11. SPONSOR/MONITOR'S REPORT NUMBER(S)

12. DISTRIBUTION/AVAILABILITY STATEMENT
Approved for public release; distribution unlimited

13. SUPPLEMENTARY NOTES

14. ABSTRACT
We generalize the recently introduced twist-Kirchhoff theory of rectangular plate elements to arbitrary quadrilateral elements. A key feature is the use of Raviart-Thomas vector-field approximations for rotations. To preserve continuity of the normal components of the rotation vector across mesh edges, we employ the Piola transformation to map the rotations from the parent domain to the physical domain. These elements possess a unique combination of efficiency and robustness in that minimal quadrature rules are sufficient to guarantee stability without rank deficiency. In particular, only one-point Gauss quadrature is required for the lowest-order element in the twist-Kirchhoff family. We numerically study the convergence and accuracy of the first two members of the twist- Kirchhoff family of quadrilateral elements on square, rhombic and circular plate problems.

15. SUBJECT TERMS

16. SECURITY CLASSIFICATION OF:			17. LIMITATION OF ABSTRACT	18. NUMBER OF PAGES	19a. NAME OF RESPONSIBLE PERSON
a. REPORT **unclassified**	b. ABSTRACT **unclassified**	c. THIS PAGE **unclassified**	**Same as Report (SAR)**	**35**	

Generalization of the Twist-Kirchhoff Theory of Plate Elements to Arbitrary Quadrilaterals and Assessment of Convergence

H.A.F.A. Santos[*], J.A. Evans[†] and T.J.R. Hughes[‡]

Institute for Computational Engineering and Sciences, The University of Texas at Austin, 201 East 24th Street, 1 University Station C0200, Austin, TX 78712, USA

Abstract

We generalize the recently introduced twist-Kirchhoff theory of rectangular plate elements to arbitrary quadrilateral elements. A key feature is the use of Raviart-Thomas vector-field approximations for rotations. To preserve continuity of the normal components of the rotation vector across mesh edges, we employ the Piola transformation to map the rotations from the parent domain to the physical domain. These elements possess a unique combination of efficiency and robustness in that minimal quadrature rules are sufficient to guarantee stability without rank deficiency. In particular, only one-point Gauss quadrature is required for the lowest-order element in the twist-Kirchhoff family. We numerically study the convergence and accuracy of the first two members of the twist-Kirchhoff family of quadrilateral elements on square, rhombic and circular plate problems.

Key words. Plates, Twist-Kirchhoff theory, Quadrilateral finite elements, Raviart-Thomas vector fields, Piola transformation.

[*]Post-doctoral Research Fellow

[†]Graduate Research Assistant

[‡]Professor of Aerospace Engineering and Engineering Mechanics, Computational and Applied Mathematics Chair III

1 Introduction

Considerable research effort has been directed toward the development of efficient and reliable quadrilateral plate finite elements. Quadrilateral elements are particularly attractive for the discretization of plates of arbitrary geometric shapes.

Most studies have been focused on the Reissner-Mindlin theory, in which transverse shear strains are accounted for. This circumvents difficulties associated with C^1 requirements of the classical Poisson-Kirchhoff theory. However, standard low-order Reissner-Mindlin-type elements suffer from shear locking when applied to thin plates. An early remedy to this was the reduced/selective integration technique [12, 11]. Unfortunately, this leads to rank deficiency and, for certain boundary conditions, to zero energy modes in excess of the three physical rigid body modes. Many research efforts have been undertaken to develop Reissner-Mindlin plate elements which have correct rank and maintain accuracy in both thin and thick plate applications, see *e.g.* [13, 14, 4, 2, 3, 7, 6, 9].

Recently, based on the so-called twist-Kirchhoff theory, which conceptually lies "in between" the classical Reissner-Mindlin and Poisson-Kirchhoff theories, a new family of rectangular plate elements has been proposed for the analysis of thin plates [8]. A salient feature of the formulation is that the mixed formulation of the lowest-order element for the limit thin-plate problem is exactly integrated with one-point Gauss quadrature. The element has no rank deficiency, and consequently does not require the stabilization of "hourglass" or any other singular modes. An "equivalent" primal element, eliminating the transverse shear force Lagrange multipliers, can be implemented by the penalty method. One-point Gauss quadrature of the primal element attains the same attributes and, in the thin plate limit, it converges to the mixed element. Consequently, one-point quadrature is also viewed as exact in this case. This element attains a combination of stability and efficiency never before achieved by a one-point quadrature quadrilateral element. Consequently, we anticipate that, when generalized to the shell setting, it may offer significant potential for economical and robust explicit crash dynamics and sheet metal forming applications. The next highest-order element shares similar properties. Its full integration rule is 2×2 Gauss quadrature. Likewise, all higher-order elements in the family behave similarly.

The unique mathematical aspect of these formulations is the use of Raviart-Thomas vector-field approximations for the rotations. We employ a Piola transformation to define the rotations in physical space for the arbitrary quadrilateral configuration. This preserves the continuity of normal rotations across element interfaces. We generalize the theory to account for the Piola transformation and show how to invoke the twist-Kirchhoff hypothesis in the arbitrary quadrilateral configuration. Based on this, we implement and numerically study the convergence behavior of the first two elements of the family in distorted configurations.

It is well known that the approximation properties of $H(\mathrm{div})$-conforming Raviart-Thomas elements deteriorate with mesh distortion [1]. In fact, there exist sequences of meshes for which the lowest-order Raviart-Thomas discretizations of the mixed Laplacian do not converge with respect to the $H(\mathrm{div})$-norm. This problem is alleviated through the utilization of higher-order Raviart-Thomas elements, albeit at the cost of a power of h. This being said, the approximation properties of lowest-order Raviart-Thomas elements remain optimal for regular families of asymptotically parallelogram meshes [5]. Furthermore, it is manifestly apparent that the lowest-order quadrilateral element may not be degenerated to a triangle in the twist-Kirchhoff theory, since in that case the transverse displacement field becomes linear in each element and the twist component of curvature, which is calculated as the mixed second-derivative of the transverse displacement, is therefore identically zero. Nevertheless, we investigate the behavior of the twist-Kirchhoff elements on highly distorted configurations, including ones in which quadrilaterals are degenerated to triangles. Indeed, for the lowest-order element, moments in degenerated triangles do not converge to correct values. However, in all other cases, the lowest-order element behaves well. The second-order element behaves well in all cases, including the case of degenerated triangles.

Square plate problems are discretized with asymptotically parallelogram-shape-regular meshes and we observe the same optimal rates of convergence for all quantities considered as observed for rectangular elements in our previous work. Convergence is also noted for the rhombic, simply-supported plate problem, known as Morley's problem, whose solution possesses singularities at the obtuse vertices. For circular plates we studied discretizations in which singularities were introduced in the geometrical mappings of elements. In every case, except for the aforementioned one, convergence was obtained for all quantities considered, even at the singularities in the geometrical mapping.

2 Twist-Kirchhoff Plate Theory

Let $\Omega \subset \mathcal{R}^2$ denote the mid-plane of a plate undergoing rotation $\boldsymbol{\theta} = [\theta_x \ \theta_y]^T$ and transverse deflection w as a result of applied distributed transverse load q and prescribed boundary rotation $\bar{\boldsymbol{\theta}}$ and deflection $\bar{w}$. Further, let $\partial\Omega = \Gamma_N \cup \Gamma_D$ denote the boundary of Ω, with Γ_N and Γ_D the Neumann and Dirichlet parts, respectively, such that $\Gamma_N \cap \Gamma_D = \varnothing$. The plate is assumed to be linear elastic, homogeneous and isotropic with Young's modulus E, Poisson's ratio ν and constant thickness t.

Let us also introduce the kinematically admissible space $\mathcal{U}$ as

$$\mathcal{U} = \{(\boldsymbol{\theta}, w) \in \mathcal{H}^1(\Omega)^2 \times \mathcal{H}^1(\Omega) |\ \boldsymbol{\theta} = \bar{\boldsymbol{\theta}} \text{ and } w = \bar{w} \text{ on } \Gamma_D\} \tag{1}$$

In the classical Reissner-Mindlin formulation, the total potential energy of the plate $\Pi_p : \mathcal{U} \to \mathcal{R}$ is given as follows

$$\Pi_p(\boldsymbol{\theta}, w) = \int_\Omega \frac{1}{2}\boldsymbol{\kappa}^T \boldsymbol{D}_M \boldsymbol{\kappa} + \frac{1}{2}\boldsymbol{\gamma}^T \boldsymbol{D}_V \boldsymbol{\gamma}\ d\Omega - \int_\Omega qw\ d\Omega \tag{2}$$

with $\boldsymbol{\kappa}$ and $\boldsymbol{\gamma}$ the curvature tensor and shear strain vector of the plate given by

$$\boldsymbol{\kappa} = \begin{bmatrix} \kappa_{xx} \\ \kappa_{yy} \\ \kappa_{xy} \end{bmatrix} = \begin{bmatrix} \theta_{x,x} \\ \theta_{y,y} \\ \theta_{x,y} + \theta_{y,x} \end{bmatrix} \quad \text{and} \quad \boldsymbol{\gamma} = \begin{bmatrix} \gamma_x \\ \gamma_y \end{bmatrix} = \begin{bmatrix} w_{,x} - \theta_x \\ w_{,y} - \theta_y \end{bmatrix} \tag{3}$$

and $\boldsymbol{D}_M$ and $\boldsymbol{D}_V$ the bending/twisting and shear constitutive matrices defined as

$$\boldsymbol{D}_M = D \begin{bmatrix} 1 & \nu & 0 \\ \nu & 1 & 0 \\ 0 & 0 & \frac{1-\nu}{2} \end{bmatrix} \quad \text{and} \quad \boldsymbol{D}_V = kGt \begin{bmatrix} 1 & 0 \\ 0 & 1 \end{bmatrix} \tag{4}$$

where $D = Et^3/(12(1-\nu^2))$, $G = E/(2(1+\nu))$ and k is the shear correction factor, usually taken to be 5/6.

The minimization of the total potential energy (2) leads to the equilibrium equations of the Reissner-Mindlin plate model.

From a numerical point of view, the difficulty with this model is the matching of the approximating spaces for $\boldsymbol{\theta}$ and w. As t tends to zero, the shear strain vector γ must tend to zero as well, *i.e.*, the shear strains $\gamma_x = w_{,x} - \theta_x$ and $\gamma_y = w_{,y} - \theta_y$ must tend to zero. If this is not allowed by the approximating spaces, the result is a deterioration of the numerical solution, well known in the literature as *shear locking*. The situation is particularly vexing if we wish to use low-order approximations.

On the other hand, finite elements based on the classical Kirchhoff theory of thin plate bending require C^1-continuity of the transverse displacement. However, whereas C^0 finite elements of various shapes and numbers of nodes are readily formulated, the construction of multidimensional C^1 elements has proven to be far more challenging.

Recently, a new theory, the *twist-Kirchhoff theory*, has been proposed for thin plates [8]. This theory lies "in between" the classical Reissner-Mindlin and Poisson-Kirchhoff theories. The main ingredient of this theory consists in replacing the Reissner-Mindlin twist component of curvature, defined in terms of first-order derivatives of the rotation components, with the classical Kirchhoff twist component of curvature, defined in terms of the second-order cross derivative of the transverse displacement, while retaining the definitions of the bending curvatures. In a rectangular Cartesian frame, this amounts to setting

$$\boldsymbol{\kappa} = \begin{bmatrix} \theta_{x,x} \\ \theta_{y,y} \\ 2w_{,xy} \end{bmatrix} \tag{5}$$

Based on this theory, a new family of rectangular displacement/rotation-based plate elements has been proposed for the analysis of thin plates [8]. This new family of elements uses $H(\text{div})$-conforming Raviart-Thomas vector fields of order $r-1$ for the rotation vector, where $r \geq 1$, standard C^0-continuous piecewise bi-Lagrange functions of order r for the transverse displacement, and an $r \times r$-point Gaussian quadrature rule for the transverse shear terms. This corresponds exactly to a mixed formulation in which the transverse shear force resultants are assumed to be discontinuous piecewise bi-Lagrange functions of order $r-1$ over each element. This family of elements has been mathematically proven to be stable, *i.e.*, possessing no hourglass modes, and to be free from shear-locking. Most notably, the lowest-order element of this family possesses only eight degrees-of-freedom, four vertex transverse displacements and four mid-side rotations, allowing exact evaluation of the stiffness matrix with one-point Gaussian quadrature.

We present in this paper the generalization of this theory to the arbitrary quadrilateral element case. This requires special treatment of the Raviart-Thomas rotation field.

Toward this end, let us first consider a nondegenerate mapping from a reference square $\widehat{K} = [-1,1]\times[-1,1]$ to a physical domain of arbitrary quadrilateral shape K as illustrated in Figure 1, where $\phi : \widehat{K} \to K$ is a regular (orientation preserving) C^1 mapping, and (x, y) and (ξ, η) denote Cartesian and curvilinear coordinates, respectively.

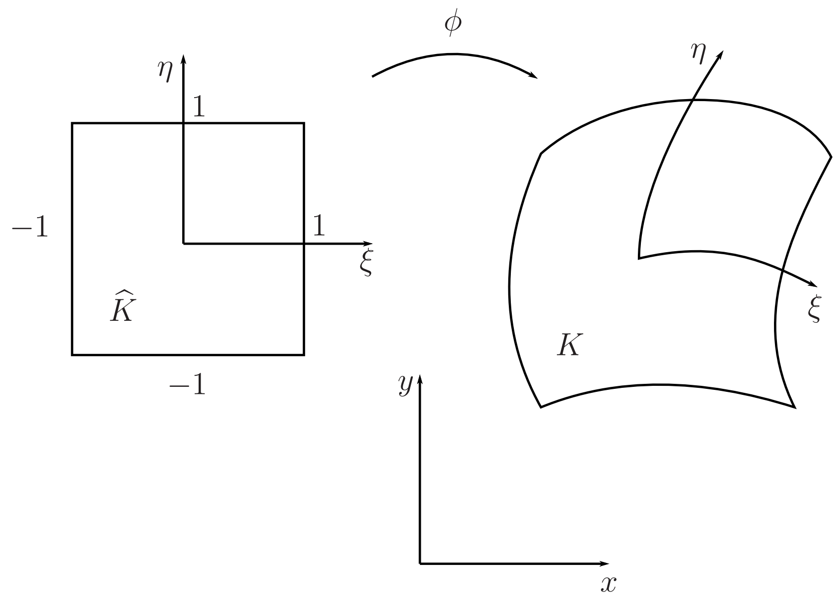

Figure 1: Geometric mapping from the parent domain to the physical domain

Further, let $\widehat{\boldsymbol{\theta}}$ be a rotation vector field on $\widehat{K}$. The Piola transform of $\widehat{\boldsymbol{\theta}}$ is given by

$$\boldsymbol{\theta} = \frac{1}{J}\boldsymbol{F}\widehat{\boldsymbol{\theta}} \tag{6}$$

where

$$\boldsymbol{\theta} = \begin{bmatrix} \theta_x \\ \theta_y \end{bmatrix}, \quad \widehat{\boldsymbol{\theta}} = \begin{bmatrix} \widehat{\theta}_\xi \\ \widehat{\theta}_\eta \end{bmatrix} \tag{7}$$

$\boldsymbol{F}$ is the Jacobian matrix of ϕ defined by

$$\boldsymbol{F} = \begin{bmatrix} x_{,\xi} & x_{,\eta} \\ y_{,\xi} & y_{,\eta} \end{bmatrix} \tag{8}$$

and $J = x_{,\xi}y_{,\eta} - x_{,\eta}y_{,\xi}$ is its determinant. The Piola transformation preserves continuity of the normal components of the rotation vector across mesh edges.

The transverse deflection is mapped using a standard push-forward with the relationship

$$w = \widehat{w} \tag{9}$$

Making use of these relations, the classical Kirchhoff assumptions, written in terms of Cartesian quantities as

$$w_{,x} - \theta_x = 0 \tag{10a}$$
$$w_{,y} - \theta_y = 0 \tag{10b}$$

can be rewritten in terms of curvilinear quantities as

$$y_{,\eta}\widehat{w}_{,\xi} - y_{,\xi}\widehat{w}_{,\eta} - x_{,\xi}\widehat{\theta}_\xi - x_{,\eta}\widehat{\theta}_\eta = 0 \tag{11a}$$
$$-x_{,\eta}\widehat{w}_{,\xi} + x_{,\xi}\widehat{w}_{,\eta} - y_{,\xi}\widehat{\theta}_\xi - y_{,\eta}\widehat{\theta}_\eta = 0 \tag{11b}$$

where we have cleared the factor of J^{-1}.

To derive the equations expressing the twist-Kirchhoff hypothesis, we first differentiate both (11a) and (11b) with respect to ξ. We then multiply the ξ-derivative of (11a) by $x_{,\eta}$, and the ξ-derivative of (11b) by $y_{,\eta}$, then we sum and solve for $\widehat{\theta}_{\eta,\xi}$. The result is (12a). We proceed in analogous fashion to obtain (12b). We differentiate (11a) and (11b) with respect to η, then we multiply the former result by $x_{,\xi}$ and the latter by $y_{,\xi}$ and sum, and solve for $\widehat{\theta}_{\xi,\eta}$, resulting in (12b).

$$\widehat{\theta}_{\eta,\xi} = A_0\big(\widehat{w}_{,\xi}A_1 + J\widehat{w}_{,\eta\xi} - \widehat{\theta}_\eta A_2 - \widehat{\theta}_{\xi,\xi}A_3 + \widehat{w}_{,\eta}A_4 - \widehat{\theta}_\xi A_5\big) \tag{12a}$$
$$\widehat{\theta}_{\xi,\eta} = B_0\big(\widehat{w}_{,\eta}B_1 + J\widehat{w}_{,\xi\eta} - \widehat{\theta}_\xi B_2 - \widehat{\theta}_{\eta,\eta}B_3 + \widehat{w}_{,\xi}B_4 - \widehat{\theta}_\eta B_5\big) \tag{12b}$$

where

$$\begin{array}{l} A_0 = 1/(x_{,\eta}^2 + y_{,\eta}^2) \\ A_1 = x_{,\eta}y_{,\xi\eta} - y_{,\eta}x_{,\xi\eta} \\ A_2 = x_{,\eta}x_{,\xi\eta} + y_{,\eta}y_{,\xi\eta} \\ A_3 = x_{,\xi}x_{,\eta} + y_{,\xi}y_{,\eta} \\ A_4 = y_{,\eta}x_{,\xi\xi} - x_{,\eta}y_{,\xi\xi} \\ A_5 = x_{,\eta}x_{,\xi\xi} + y_{,\eta}y_{,\xi\xi} \end{array} \quad \text{and} \quad \begin{array}{l} B_0 = 1/(x_{,\xi}^2 + y_{,\xi}^2) \\ B_1 = y_{,\xi}x_{,\xi\eta} - x_{,\xi}y_{,\xi\eta} \\ B_2 = x_{,\xi}x_{,\xi\eta} + y_{,\xi}y_{,\xi\eta} \\ B_3 = x_{,\xi}x_{,\eta} + y_{,\xi}y_{,\eta} \\ B_4 = x_{,\xi}y_{,\eta\eta} - y_{,\xi}x_{,\eta\eta} \\ B_5 = x_{,\xi}x_{,\eta\eta} + y_{,\xi}y_{,\eta\eta} \end{array} \tag{13}$$

Equations (12a) and (12b) represent the twist-Kirchhoff assumptions for the general quadrilateral element defined in the curvilinear system (ξ, η). See Figure 1. Note that, in the rectangular case, (12a) and (12b) simplify to

$$\widehat{\theta}_{\eta,\xi} = \widehat{w}_{,\eta\xi} \tag{14a}$$
$$\widehat{\theta}_{\xi,\eta} = \widehat{w}_{,\xi\eta} \tag{14b}$$

Further, the derivatives of the Cartesian components of the rotation vector with respect to the Cartesian coordinates can be expressed in terms of their corresponding curvilinear components as follows

$$\theta_{x,x} = J^{-2}\big((C_1 - D_1)y_{,\eta} - (C_2 - D_2)y_{,\xi}\big) \tag{15a}$$
$$\theta_{y,y} = J^{-2}\big((C_4 - D_4)x_{,\xi} - (C_3 - D_3)x_{,\eta}\big) \tag{15b}$$
$$\theta_{x,y} = J^{-2}\big((C_2 - D_2)x_{,\xi} - (C_1 - D_1)x_{,\eta}\big) \tag{15c}$$
$$\theta_{y,x} = J^{-2}\big((C_3 - D_3)y_{,\eta} - (C_4 - D_4)y_{,\xi}\big) \tag{15d}$$

with

$$
\begin{aligned}
C_1 &= x_{,\xi}\widehat{\theta}_{\xi,\xi} + x_{,\eta}\widehat{\theta}_{\eta,\xi} \\
C_2 &= x_{,\xi}\widehat{\theta}_{\xi,\eta} + x_{,\eta}\widehat{\theta}_{\eta,\eta} \\
C_3 &= y_{,\xi}\widehat{\theta}_{\xi,\xi} + y_{,\eta}\widehat{\theta}_{\eta,\xi} \\
C_4 &= y_{,\xi}\widehat{\theta}_{\xi,\eta} + y_{,\eta}\widehat{\theta}_{\eta,\eta}
\end{aligned}
\quad \text{and} \quad
\begin{aligned}
D_1 &= J^{-1}(A_4 - B_1)E_1 - x_{,\xi\eta}\widehat{\theta}_{\eta} - x_{,\xi\xi}\widehat{\theta}_{\xi} \\
D_2 &= J^{-1}(B_4 - A_1)E_1 - x_{,\xi\eta}\widehat{\theta}_{\xi} - x_{,\eta\eta}\widehat{\theta}_{\eta} \\
D_3 &= J^{-1}(A_4 - B_1)E_2 - y_{,\xi\eta}\widehat{\theta}_{\eta} - y_{,\xi\xi}\widehat{\theta}_{\xi} \\
D_4 &= J^{-1}(B_4 - A_1)E_2 - y_{,\xi\eta}\widehat{\theta}_{\xi} - y_{,\eta\eta}\widehat{\theta}_{\eta}
\end{aligned}
\tag{16}
$$

where

$$
\begin{aligned}
E_1 &= x_{,\xi}\widehat{\theta}_{\xi} + x_{,\eta}\widehat{\theta}_{\eta} \\
E_2 &= y_{,\xi}\widehat{\theta}_{\xi} + y_{,\eta}\widehat{\theta}_{\eta}
\end{aligned}
\tag{17}
$$

Finally, by invoking the twist-Kirchhoff assumptions (12a) and (12b), and substituting them into (15a)-(15d), we obtain the components of the twist-Kirchhoff curvature vector for the arbitrary quadrilateral element case as

$$\kappa_{xx} = J^{-2}\big((C_1 - D_1)y_{,\eta} - (C_2 - D_2)y_{,\xi}\big) \tag{18a}$$

$$\kappa_{yy} = J^{-2}\big((C_4 - D_4)x_{,\xi} - (C_3 - D_3)x_{,\eta}\big) \tag{18b}$$

$$\kappa_{xy} = J^{-2}\big((C_2 - D_2)x_{,\xi} - (C_1 - D_1)x_{,\eta} + (C_3 - D_3)y_{,\eta} - (C_4 - D_4)y_{,\xi}\big) \tag{18c}$$

where the variables C_1, C_2, C_3 and C_4 are redefined as

$$
\begin{aligned}
C_1 &= x_{,\xi}\widehat{\theta}_{\xi,\xi} + x_{,\eta}A_0\big(\widehat{w}_{,\xi}A_1 + J\widehat{w}_{,\eta\xi} - \widehat{\theta}_{\eta}A_2 - \widehat{\theta}_{\xi,\xi}A_3 + \widehat{w}_{,\eta}A_4 - \widehat{\theta}_{\xi}A_5\big) \\
C_2 &= x_{,\xi}B_0\big(\widehat{w}_{,\eta}B_1 + J\widehat{w}_{,\xi\eta} - \widehat{\theta}_{\xi}B_2 - \widehat{\theta}_{\eta,\eta}B_3 + \widehat{w}_{,\xi}B_4 - \widehat{\theta}_{\eta}B_5\big) + x_{,\eta}\widehat{\theta}_{\eta,\eta} \\
C_3 &= y_{,\xi}\widehat{\theta}_{\xi,\xi} + y_{,\eta}A_0\big(\widehat{w}_{,\xi}A_1 + J\widehat{w}_{,\eta\xi} - \widehat{\theta}_{\eta}A_2 - \widehat{\theta}_{\xi,\xi}A_3 + \widehat{w}_{,\eta}A_4 - \widehat{\theta}_{\xi}A_5\big) \\
C_4 &= y_{,\xi}B_0\big(\widehat{w}_{,\eta}B_1 + J\widehat{w}_{,\xi\eta} - \widehat{\theta}_{\xi}B_2 - \widehat{\theta}_{\eta,\eta}B_3 + \widehat{w}_{,\xi}B_4 - \widehat{\theta}_{\eta}B_5\big) + y_{,\eta}\widehat{\theta}_{\eta,\eta}
\end{aligned}
\tag{19}
$$

3 Finite Element Approximations

In the parent domain, the rotations are represented by $H(\text{div})$-conforming Raviart-Thomas vector fields of order $r-1$, where $r \geq 1$, and the transverse displacement is represented by standard C^0-continuous, piecewise bi-Lagrange functions of order r. Similarly to the rectangular element case, numerical stability in the arbitrary quadrilateral element case requires the use of an $r \times r$-point Gaussian rule on the transverse shear term. We note that, in the rectangular case, the $r \times r$-point Gaussian rule is exact for the bending term. The first two members of the family of elements, defined in the parent domain, are schematically illustrated in Figure 2.

For the first- and second-order elements, *i.e.*, for $r = 1$ and $r = 2$, the rotation components and the transverse displacement fields in the parametric coordinates are expressed as

$$
\begin{aligned}
\widehat{\theta}^h_{\xi} &= \sum_{i=1}^{2} \widehat{N}_i^{\theta_\xi}\theta_i^{\xi} \\
\widehat{\theta}^h_{\eta} &= \sum_{i=1}^{2} \widehat{N}_i^{\theta_\eta}\theta_i^{\eta} \\
\widehat{w}^h &= \sum_{i=1}^{4} \widehat{N}_i^{w} w_i
\end{aligned}
\quad \text{and} \quad
\begin{aligned}
\widehat{\theta}^h_{\xi} &= \sum_{i=1}^{6} \widehat{N}_i^{\theta_\xi}\theta_i^{\xi} \\
\widehat{\theta}^h_{\eta} &= \sum_{i=1}^{6} \widehat{N}_i^{\theta_\eta}\theta_i^{\eta} \\
\widehat{w}^h &= \sum_{i=1}^{9} N_i^{w} w_i
\end{aligned}
\tag{20}
$$

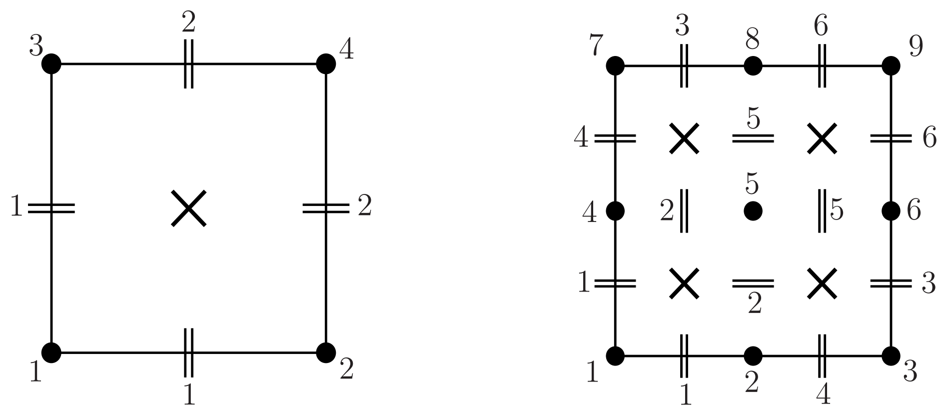

(a) $r = 1$ (b) $r = 2$

Figure 2: First two members of the element family

● w^h degree of freedom

═ θ_ξ^h degree of freedom

‖ θ_η^h degree of freedom

× Quadrature points

respectively, where θ_i^ξ and θ_i^η represent mid-side rotational degrees-of-freedom about the η- and ξ-constant coordinate lines, respectively, whereas w_i represent vertex displacement degrees-of-freedom, as illustrated in Figure 2. Note that, in the physical domain, the rotational degrees-of-freedom become the normal components of the rotation on the element boundaries.

In the first-order element, the shape functions for the rotations and transverse displacement defined in parametric coordinates are

$$\begin{array}{ll} \widehat{N}_1^{\theta_\xi} = \frac{1}{2}(1-\xi) & \widehat{N}_1^{w} = \frac{1}{4}(1-\xi)(1-\eta) \\ \widehat{N}_2^{\theta_\xi} = \frac{1}{2}(1+\xi) & \widehat{N}_2^{w} = \frac{1}{4}(1+\xi)(1-\eta) \\ \widehat{N}_1^{\theta_\eta} = \frac{1}{2}(1-\eta) & \widehat{N}_3^{w} = \frac{1}{4}(1-\xi)(1+\eta) \\ \widehat{N}_2^{\theta_\eta} = \frac{1}{2}(1+\eta) & \widehat{N}_4^{w} = \frac{1}{4}(1+\xi)(1+\eta) \end{array} \tag{21}$$

whereas in the second-order element they are

$$\begin{array}{ll} \widehat{N}_1^{\theta_\xi} = \frac{1}{4}\xi(\xi-1)(1-\eta) & \\ \widehat{N}_2^{\theta_\xi} = \frac{1}{2}(1-\xi^2)(1-\eta) & \\ \widehat{N}_3^{\theta_\xi} = \frac{1}{4}\xi(\xi+1)(1-\eta) & \widehat{N}_1^{w} = \frac{1}{4}\xi\eta(1-\xi)(1-\eta) \\ \widehat{N}_4^{\theta_\xi} = \frac{1}{4}\xi(\xi-1)(1+\eta) & \widehat{N}_2^{w} = -\frac{1}{2}\eta(1-\eta)(1-\xi^2) \\ \widehat{N}_5^{\theta_\xi} = \frac{1}{2}(1-\xi^2)(1+\eta) & \widehat{N}_3^{w} = -\frac{1}{4}\xi\eta(1+\xi)(1-\eta) \\ \widehat{N}_6^{\theta_\xi} = \frac{1}{4}\xi(\xi+1)(1+\eta) & \widehat{N}_4^{w} = -\frac{1}{2}\xi(1-\xi)(1-\eta^2) \\ \widehat{N}_1^{\theta_\eta} = \frac{1}{4}\eta(1-\xi)(\eta-1) & \widehat{N}_5^{w} = (1-\xi^2)(1-\eta^2) \\ \widehat{N}_2^{\theta_\eta} = \frac{1}{2}(1-\xi)(1-\eta^2) & \widehat{N}_6^{w} = \frac{1}{2}\xi(1+\xi)(1-\eta^2) \\ \widehat{N}_3^{\theta_\eta} = \frac{1}{4}\eta(1-\xi)(\eta+1) & \widehat{N}_7^{w} = -\frac{1}{4}\xi\eta(1-\xi)(1+\eta) \\ \widehat{N}_4^{\theta_\eta} = \frac{1}{4}\eta(1+\xi)(\eta-1) & \widehat{N}_8^{w} = \frac{1}{2}\eta(1+\eta)(1-\xi^2) \\ \widehat{N}_5^{\theta_\eta} = \frac{1}{2}(1+\xi)(1-\eta^2) & \widehat{N}_9^{w} = \frac{1}{4}\xi\eta(1+\xi)(1+\eta) \\ \widehat{N}_6^{\theta_\eta} = \frac{1}{4}\eta(1+\xi)(\eta+1) & \end{array} \tag{22}$$

4 Numerical Results

We use the primal formulation with a reduced quadrature rule; see [8] for further details. For the first-order element we use a one-point Gaussian quadrature rule, whereas for the second-order element we use a 2×2-point tensor-product Gaussian quadrature rule. To analyze the effectiveness of the elements, we computed solutions for the first- and second-order cases for thicknesses of 0.01, 0.001, and 0.0001. For all computations, a shear correction factor of 5/6 is utilized to achieve results that are consistent with classical bending theory [10]. All the examples refer to isotropic plates with Young's modulus and Poisson's ratio taken as $E = 10^7$ and $\nu = 0.3$. A uniform distributed load of magnitude $q = 1$ is applied in all cases. The specification of essential boundary conditions is identical to that of Poisson-Kirchhoff theory, *i.e.*, for simply-supported edges we only impose $w = 0$, for clamped edges we impose $w = 0$ and $\theta_n = 0$. The geometrical map of the element utilizes the same basis functions as those for the transverse displacement.

The energy errors presented are computed with the bending strain energy norm, defined as

$$\|\boldsymbol{\kappa}\| = \left(\frac{1}{2}\int_{\Omega} \boldsymbol{\kappa}^T \boldsymbol{D}_M \boldsymbol{\kappa}\, d\Omega\right)^{\frac{1}{2}} \tag{23}$$

As proven in [8], for the first-order rectangular element we have second-order convergence for w in $L^2(\Omega)$, first-order convergence for w in $H^1(\Omega)$, and first-order convergence for $\|\boldsymbol{\kappa}\|$, while for the second-order rectangular element we have third-order convergence for w in $L^2(\Omega)$, second-order convergence for w in $H^1(\Omega)$, and second-order convergence for $\|\boldsymbol{\kappa}\|$. As will be shown next, there is no degradation of these orders of convergence when using asymptotically parallelogram-shape-regular meshes, *i.e.*, meshes whose elements converge to parallelograms in the limit of mesh refinement and whose element aspect ratios are uniformly bounded from above and below.

4.1 Square Plate

We consider an isotropic square plate subject to uniform loading. The simply-supported case is presented in Section 4.1.1 and the fully-clamped case is analyzed in Section 4.1.2.

The adopted refinement scheme consists of "uniform" refinements of a non-uniform mesh obtained by splitting the square into four quadrilaterals, as illustrated in Figure 3, where D_p represents the distortion parameter. In the present case, D_p was set to 1/10. Each refinement step is obtained by subdividing each quadrilateral into four elements by connecting the midpoints of the opposite edges. This leads to a family of $n_{el} \times n_{el}$ asymptotically parallelogram-shape-regular meshes as shown in Figure 4 for the first three meshes.

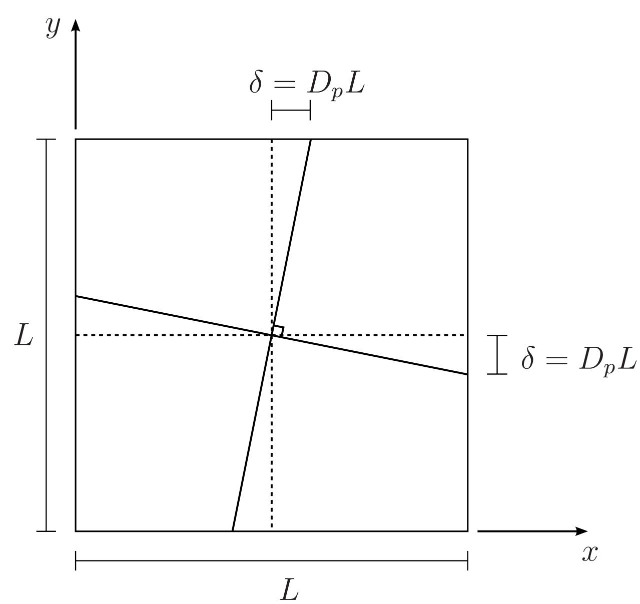

Figure 3: First mesh for square plate problem - distortion parameter

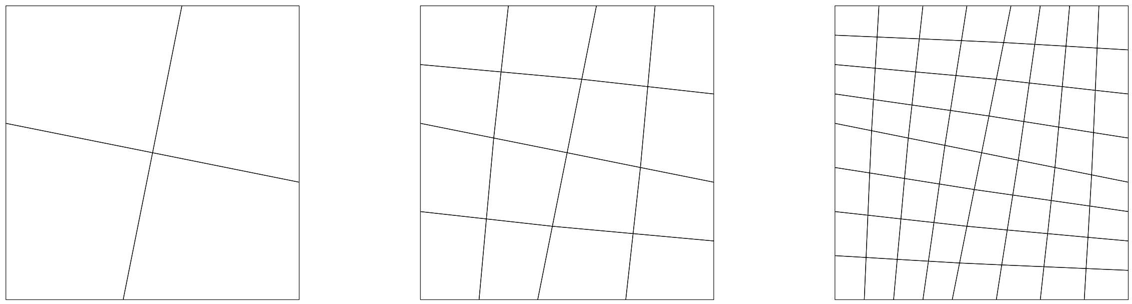

(a) $n_{el} = 2$ (b) $n_{el} = 4$ (c) $n_{el} = 8$

Figure 4: Asymptotically parallelogram meshes for square plate problem

4.1.1 Simply-Supported Case

Let us consider the simply-supported square plate illustrated in Figure 5.

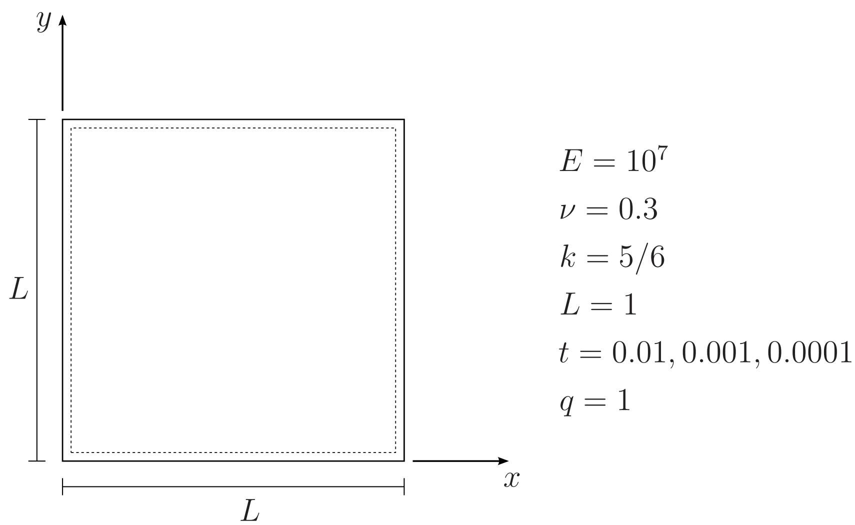

Figure 5: Simply-supported square plate model

We first study convergence rates. Since there is no known analytical solution to the twist-Kirchhoff problem, we compare discrete solutions with a heavily refined (128×128 mesh) solution with the second-order element. We use this to determine *rates* of convergence in integral norms. That we are converging to the *exact* solution will be verified by tabular results presented subsequently. We present the global error as measured by the bending strain energy norm obtained for the thickness case $t = 0.001$ in Figure 6. Similarly, we present the displacement errors as measured by the L^2 and H^1 norms in Figures 7(a) and 7(b), respectively. The plotted errors are normalized by the norms of the reference solution. Examining these figures, we observe rates of convergence for both the first- and the second-order element cases which are the same as the optimal rates of

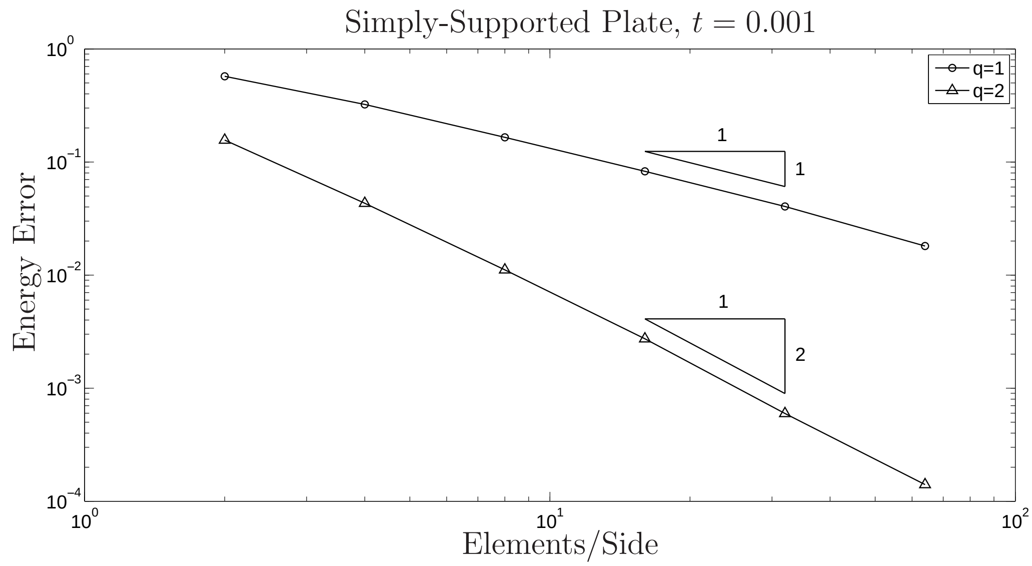

Figure 6: The normalized total error produced by the lowest- and second-order plate elements for the simply-supported square plate under a uniform load for a thickness value of 0.001.

convergence for the rectangular element case.

We now study the convergence of the center displacement. Tables 1 and 2 display the convergence of the center displacement for the first- and second-order plate elements respectively. The displayed center displacements are scaled by $10^3 D/(qL^4)$. Comparing our converged twist-Kirchhoff results with the reference Poisson-Kirchhoff solution [20], we find the twist-Kirchhoff center displacement converges to the thin plate displacement from above as the thickness/width ratio $t/L \to 0$, as we might have anticipated. To compare our twist-Kirchhoff results with Reissner-Mindlin theory, we have simulated a simply-supported Reissner-Mindlin plate using 256×256 quadratic Lagrange rectangular elements and selective reduced integration [11]. Table 3 displays the computed center displacements, which we have confirmed are converged to five significant digits. We find the converged twist-Kirchhoff displacements from Tables 1 and 2 lie below the corresponding Reissner-Mindlin displacements for a fixed thickness/length ratio t/L. This result also seems consistent with the "in between" nature of the twist-Kichhoff theory.

We next study the convergence of the center bending moment about the x-axis. Since the discrete center bending moment is not well-defined, we sample it at a quadrature point lying closest to the center of the plate. Tables 4 and 5 display the convergence of the center moments for the first- and second-order plate elements, respectively. The displayed center moments are scaled by $10^2/(qL^2)$. As expected, the convergence rate for the bending moment is slower than that for the center displacement. This is significantly influenced by the fact that the location at which we sample the bending moment within an element is $O(h)$, where $h \approx 1/n_{el}$, and thus we would have no reason to expect convergence to

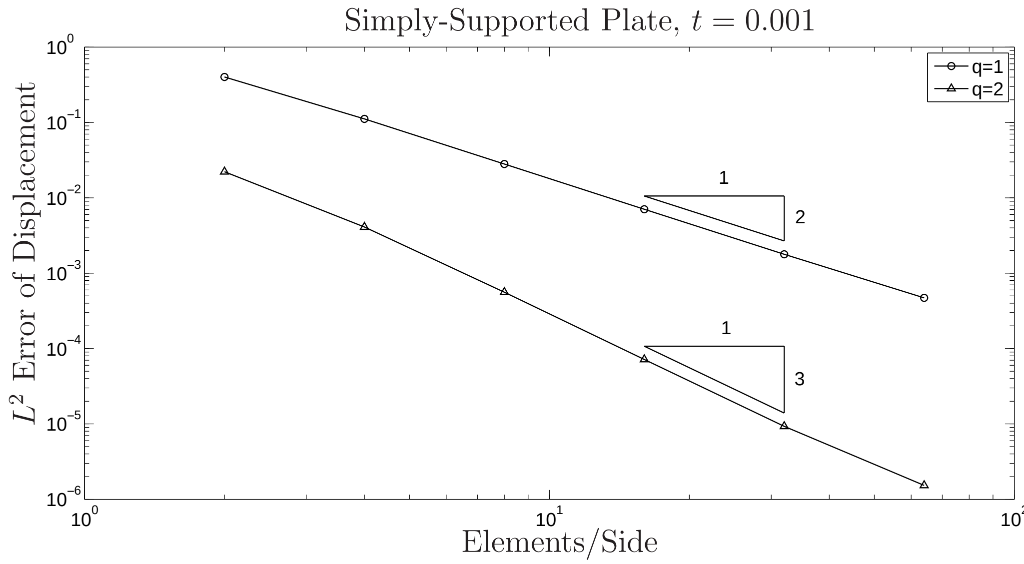

(a)

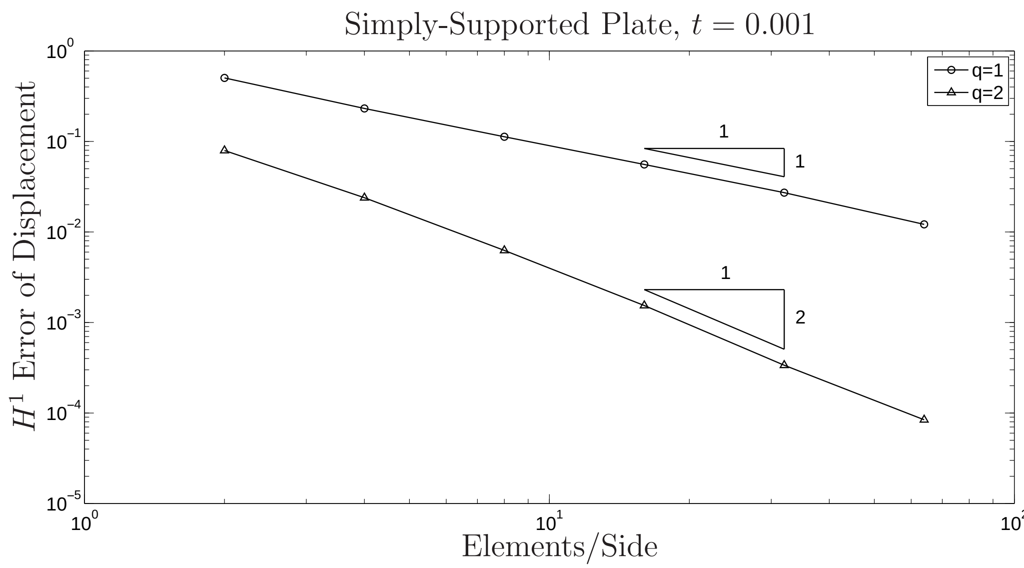

(b)

Figure 7: (a) The normalized L^2 norm of the displacement produced by the lowest- and second-order plate elements for the simply-supported square plate under a uniform load for a thickness value of 0.001. (b) The normalized H^1 norm of the displacement for the same problem.

Mesh	$t/L = 0.01$	$t/L = 0.001$	$t/L = 0.0001$
2×2	3.86286	3.86128	3.86126
4×4	4.08572	4.08479	4.08479
8×8	4.07035	4.06952	4.06951
16×16	4.06500	4.06416	4.06415
32×32	4.06366	4.06281	4.06280
64×64	4.06332	4.06247	4.06247

Table 1: Center displacement ($w \times 10^3 D/(qL^4)$) for first-order element simply-supported square plate solutions for the three thickness/length ratios. Reference thin plate limit solution is 4.06235 [20].

Mesh	$t/L = 0.01$	$t/L = 0.001$	$t/L = 0.0001$
2×2	4.20035	4.19957	4.19956
4×4	4.07131	4.07050	4.07049
8×8	4.06369	4.06286	4.06285
16×16	4.06323	4.06239	4.06238
32×32	4.06321	4.06236	4.06235
64×64	4.06321	4.06236	4.06235

Table 2: Center displacement ($w \times 10^3 D/(qL^4)$) for second-order element simply-supported square plate solutions for the three thickness/length ratios. Reference thin plate limit solution is 4.06235 [20].

$t/L = 0.01$	$t/L = 0.001$	$t/L = 0.0001$
4.09930	4.06585	4.06268

Table 3: Center displacement ($w \times 10^3 D/(qL^4)$) for simply-supported Reissner-Mindlin plate. Computed using 256×256 quadratic Lagrange rectangular elements and selective reduced integration [11].

Mesh	$t/L = 0.01$	$t/L = 0.001$	$t/L = 0.0001$
2×2	1.88468	1.88516	1.88517
4×4	4.17328	4.17385	4.17385
8×8	4.64061	4.64103	4.64104
16×16	4.75203	4.75238	4.75238
32×32	4.77916	4.77969	4.77968
64×64	4.78584	4.78643	4.78641

Table 4: "Center" bending moment about the x-axis ($M_x \times 10^2/(qL^2)$) for first-order element simply-supported square plate solutions for the three thickness/length ratios. Reference thin plate limit solution is 4.78864 [20].

Mesh	$t/L = 0.01$	$t/L = 0.001$	$t/L = 0.0001$
2×2	4.52602	4.52648	4.52649
4×4	4.68831	4.68874	4.68875
8×8	4.76160	4.76167	4.76167
16×16	4.78166	4.78171	4.78170
32×32	4.78646	4.78694	4.78688
64×64	4.78765	4.78823	4.78820

Table 5: "Center" bending moment about the x-axis ($M_x \times 10^2/(qL^2)$) for second-order element simply-supported square plate solutions for the three thickness/length ratios. Reference thin plate limit solution is 4.78864 [20].

be any better than first-order. However, we observe second-order convergence for both elements, with the absolute values of the error being more accurate for the second-order element.

4.1.2 Fully-Clamped Case

Let us now consider the case of a fully-clamped square plate, as illustrated in Figure 8.

In Figure 9 we present the global error as measured by the bending strain energy norm. Similarly, we present the displacement errors as measured by the L^2 and H^1 norms in Figures 10(a) and 10(b), respectively. The plotted errors are normalized by the norms of the exact solution. As in the simply-supported plate problem, we observe no degradation of the optimal rates of convergence for the rectangular element case.

Tables 6 and 7 display the convergence of the center displacement for the first- and second-order plate elements, respectively. As can be seen, the twist-Kirchhoff center displacement converges to the thin plate displacement from above as the thickness/length ratio $t/L \to 0$. To compare our twist-Kirchhoff results with Reissner-Mindlin theory, we simulated a clamped Reissner-Mindlin plate using 256×256 quadratic Lagrange rect-

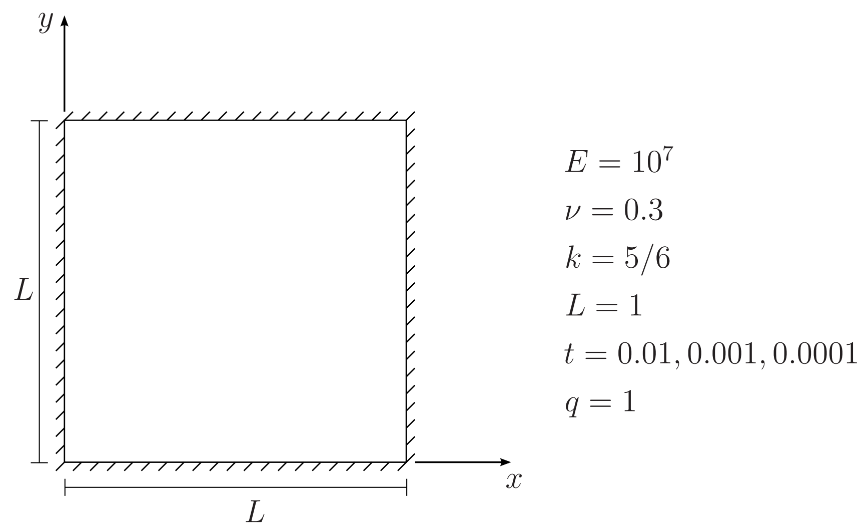

Figure 8: Fully-clamped square plate model

Mesh	$t/L = 0.01$	$t/L = 0.001$	$t/L = 0.0001$
2×2	0.00343	0.00003	0.00000
4×4	1.21557	1.21318	1.21316
8×8	1.26333	1.26139	1.26137
16×16	1.26653	1.26471	1.26469
32×32	1.26700	1.26520	1.26518
64×64	1.26710	1.26530	1.26529

Table 6: Center displacement $(w \times 10^3 D/(qL^4))$ for first-order element fully-clamped square plate solutions for the three thickness/length ratios. Reference thin plate limit solution is 1.26532 [19].

angular elements and selective reduced integration [11]. Table 8 displays the computed center displacements, which we have confirmed are converged to six significant digits. As was the case for the simply-supported plate, we find the converged twist-Kirchhoff displacements lie below the corresponding Reissner-Mindlin displacements for a fixed thickness/length ratio t/L. This result again seems consistent with the “in between” nature of the twist-Kichhoff theory.

We next study the convergence of the center bending moment about the x-axis. As was done for the simply-supported case, we sample the discrete bending moment at a quadrature point lying closest to the center of the plate. Tables 9 and 10 display the convergence of the center moment for the first- and second-order plate elements, respectively. The displayed center moments are scaled by $10^2/(qL^2)$. We note that the bending moment exhibits second-order convergence for both the first- and second-order case, but with the second-order case being more accurate on an absolute basis.

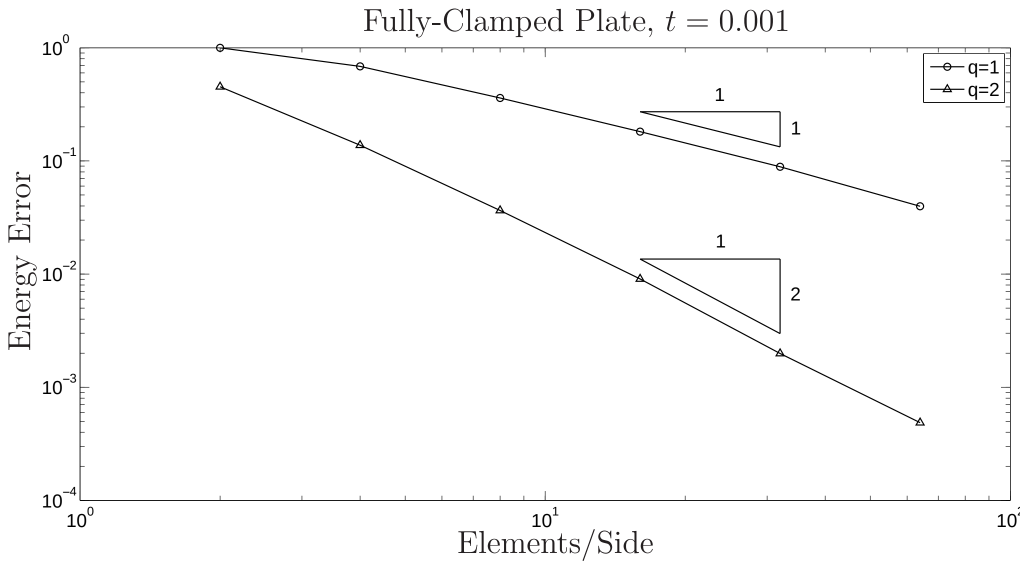

Figure 9: The normalized total error produced by the lowest- and second-order plate elements for the fully-clamped isotropic plate under a uniform load for a thickness value of 0.001.

Mesh	$t/L = 0.01$	$t/L = 0.001$	$t/L = 0.0001$
2×2	1.50167	1.49994	1.49992
4×4	1.27850	1.27664	1.27662
8×8	1.26785	1.26603	1.26601
16×16	1.26718	1.26538	1.26536
32×32	1.26714	1.26534	1.26532
64×64	1.26714	1.26534	1.26532

Table 7: Center displacement ($w \times 10^3 D/(qL^4)$) for second-order element fully-clamped square plate solutions for the three thickness/length ratios. Reference thin plate limit solution is 1.26532 [19].

$t/L = 0.01$	$t/L = 0.001$	$t/L = 0.0001$
1.26787	1.26534	1.26532

Table 8: Center displacement ($w \times 10^3 D/(qL^4)$) for clamped Reissner-Mindlin plate. Computed using 256×256 quadratic Lagrange rectangular elements and selective reduced integration [11].

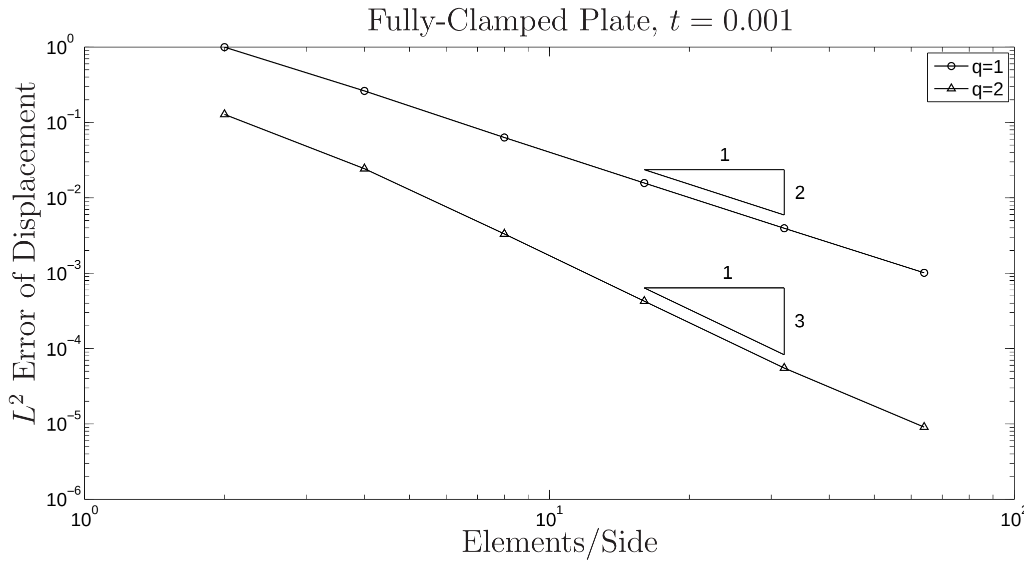

(a)

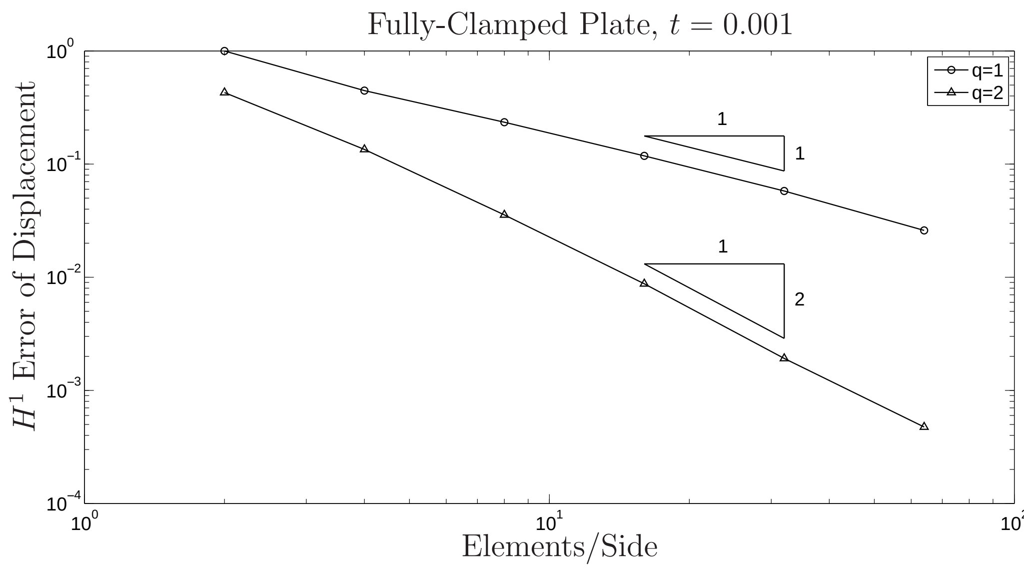

(b)

Figure 10: (a) The normalized L^2 norm of the displacement produced by the lowest- and second-order plate elements for the fully-clamped isotropic plate under a uniform load for a thickness value of 0.001. (b) The normalized H^1 norm of the displacement for the same problem.

Mesh	$t/L = 0.01$	$t/L = 0.001$	$t/L = 0.0001$
2×2	-0.00019	0.00000	0.00000
4×4	2.05023	2.05186	2.05188
8×8	2.22775	2.23134	2.23138
16×16	2.27135	2.27615	2.27630
32×32	2.28529	2.28656	2.28701
64×64	2.28903	2.28928	2.28962

Table 9: "Center" bending moment about the x-axis ($M_x \times 10^2/(qL^2)$) for first-order element fully-clamped square plate solutions for the three thickness/length ratios. Reference thin plate limit solution is 2.29051 [19].

Mesh	$t/L = 0.01$	$t/L = 0.001$	$t/L = 0.0001$
2×2	1.96176	1.96023	1.96022
4×4	2.16743	2.16461	2.16458
8×8	2.26193	2.25608	2.25595
16×16	2.28422	2.28206	2.28161
32×32	2.28879	2.28881	2.28828
64×64	2.28990	2.29013	2.29000

Table 10: "Center" bending moment about the x-axis ($M_x \times 10^2/(qL^2)$) for second-order element fully-clamped square plate solutions for the three thickness/length ratios. Reference thin plate limit solution is 2.29051 [19].

4.2 Simply-Supported Morley's Plate

Let us now consider an isotropic simply-supported rhombic plate under uniform transverse loading as illustrated in Figure 11. In this case, a singular behaviour is known to occur at the obtuse vertices. As a result, we anticipate some difficulties may arise. In fact, some thin plate elements yield pathological results for this problem [18]. An analytical solution given as an infinite series was obtained in [15] for the Poisson-Kirchhoff case.

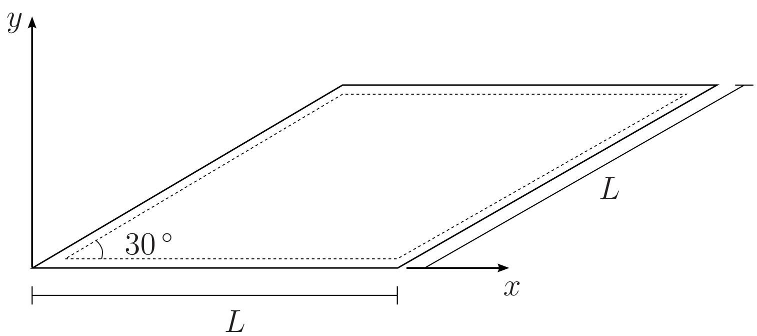

$E = 10^7$

$\nu = 0.3$

$k = 5/6$

$L = 1$

$t = 0.01, 0.001, 0.0001$

$q = 1$

Figure 11: Simply-supported Morley's plate model

The adopted refinement scheme consists in uniform $n_{el} \times n_{el}$ parallelogram-shape-regular meshes as shown in Figure 12 for the first three meshes.

We first study the convergence of the center displacement. Tables 11 and 12 display the convergence of the center displacement for the first- and second-order plate elements, respectively. Comparing our converged twist-Kirchhoff results with the reference Poisson-Kirchhoff solution [15] evaluated retaining nine terms of the infinite series, we find the twist-Kirchhoff center displacement converges to the thin plate displacement from above as the thickness/length ratio $t/L \to 0$.

We next study the convergence of the maximum and minimum principal center bending moments. We sample the discrete bending moment at a quadrature point lying closest to the center of the plate. Tables 13 and 14 display the convergence of the center bending moments for the first- and second-order elements, respectively. The displayed center moments are scaled by $10^2/(qL^2)$. We note that the bending moment converges slowly for both the first- and second-order cases. The second-order discretization is slightly

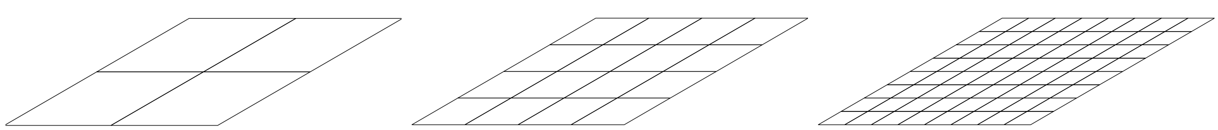

(a) $n_{el} = 2$ (b) $n_{el} = 4$ (c) $n_{el} = 8$

Figure 12: Parallelogram meshes for Morley's plate problem

Mesh	$t/L = 0.01$	$t/L = 0.001$	$t/L = 0.0001$
2×2	0.26392	0.26307	0.26306
4×4	0.43539	0.43473	0.43472
8×8	0.43717	0.43675	0.43674
16×16	0.42091	0.41935	0.41933
32×32	0.41810	0.41325	0.41307
64×64	0.41794	0.41177	0.41066
128×128	0.41790	0.41170	0.40958

Table 11: Center displacement ($w \times 10^3 D/(qL^4)$) for first-order element simply-suported Morley's plate solutions for the three thickness/length ratios. Reference thin plate limit solution evaluated retaining nine terms in the series is 0.40777 [15].

Mesh	$t/L = 0.01$	$t/L = 0.001$	$t/L = 0.0001$
2×2	0.50100	0.50035	0.50034
4×4	0.44586	0.44545	0.44544
8×8	0.42174	0.42064	0.42063
16×16	0.41799	0.41379	0.41367
32×32	0.41790	0.41182	0.41098
64×64	0.41789	0.41169	0.40972
128×128	0.41789	0.41169	0.40939

Table 12: Center displacement ($w \times 10^3 D/(qL^4)$) for second-order element simply-supported Morley's plate solutions for the three thickness/length ratios. Reference thin plate limit solution evaluated retaining nine terms in the series is 0.40777 [15].

more accurate in absolute terms. These low rates of convergence can be attributed to the singularities at the obtuse corners, and the fact that the meshes are uniform and not graded to better represent the singular behavior.

4.3 Circular Plate

Let us now consider an isotropic circular plate under uniform transverse loading. As in the square plate problem, we analyze both the simply-supported and the fully-clamped cases; see Sections 4.3.1 and 4.3.2, respectively.

Two different mesh refinement schemes are adopted in this case. One is based on a sequence of polar meshes (PM), whereas the other is based on a sequence of meshes obtained by mapping a square domain onto a circle (SCM). We note that for the PM-meshes, we can interpret the triangular elements around the center as degenerate quadrilaterals with one edge collapsed. Hence, from the computational point of view, for the coincident nodes, the associated degrees-of-freedom were made equivalent, while the rotational

	$t/L = 0.01$		$t/L = 0.001$		$t/L = 0.0001$	
Mesh	M_{max}	M_{min}	M_{max}	M_{min}	M_{max}	M_{min}
2×2	0.80932	0.19377	0.80935	0.19410	0.80935	0.19410
4×4	1.67762	0.47686	1.67774	0.47685	1.67774	0.47685
8×8	1.93080	0.76694	1.93162	0.76060	1.93163	0.76054
16×16	1.94468	0.97043	1.95618	0.90315	1.95637	0.90218
32×32	1.93018	1.10883	1.94570	0.97020	1.94832	0.95879
64×64	1.93288	1.11883	1.92356	1.06029	1.93762	0.99155
128×128	1.93374	1.12036	1.91706	1.09950	1.92559	1.02745

Table 13: Maximum and minimum principal "center" bending moments ($M \times 10^2/(qL^2)$) for first-order element simply-supported Morley's plate solutions for the three thickness/length ratios. Reference thin plate limit solutions evaluated retaining nine terms in the series are 1.9080 and 1.0834 [15].

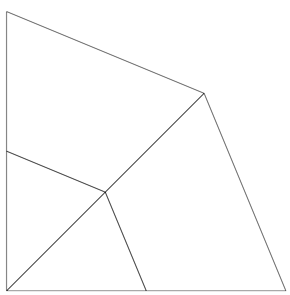

(a) $n_{el} = 2$

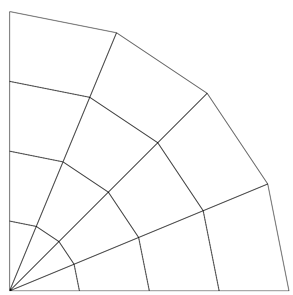

(b) $n_{el} = 4$

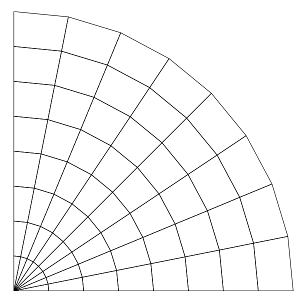

(c) $n_{el} = 8$

Figure 13: PM meshes with bi-linear mapping for circular plate problem

degrees-of-freedom associated with collapsed edges were removed from the system, *i.e.*, set to zero. We are particularly interested in the effect of degenerating the elements on local derivative quantities, especially the bending moments.

For the PM-meshes we exploit symmetry conditions and only discretize the first quadrant of the plate, whereas for the SCM-meshes we discretize the whole domain, see Figures 13 and 14, respectively. n_{el} represents in this case the adopted number of elements per side in one quadrant of the plate. For the meshes with second-order elements we use a geometrical bi-quadratic mapping, in which initially straight edges in the reference domain are mapped onto curved edges in the physical domain; see Figures 15 and 16. As mentioned in Section 1, we have no illusions about the lowest-order twist-Kirchhoff element being able to deal with polar meshes.

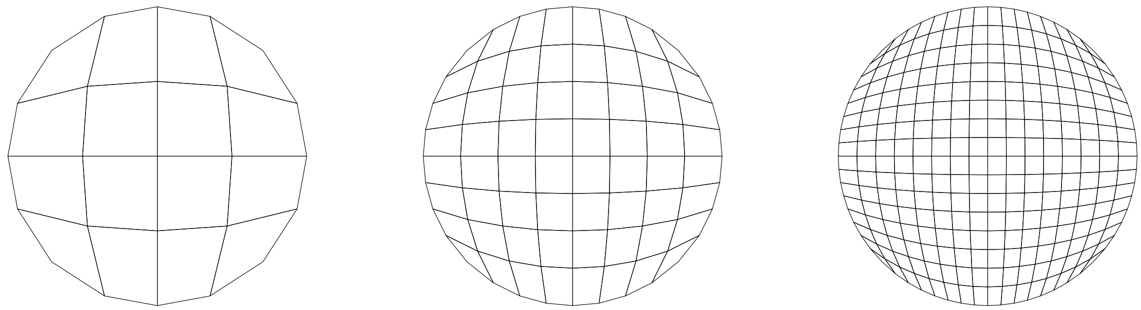

(a) $n_{el} = 2$ (b) $n_{el} = 4$ (c) $n_{el} = 8$

Figure 14: SCM meshes with bi-linear mapping for circular plate problem

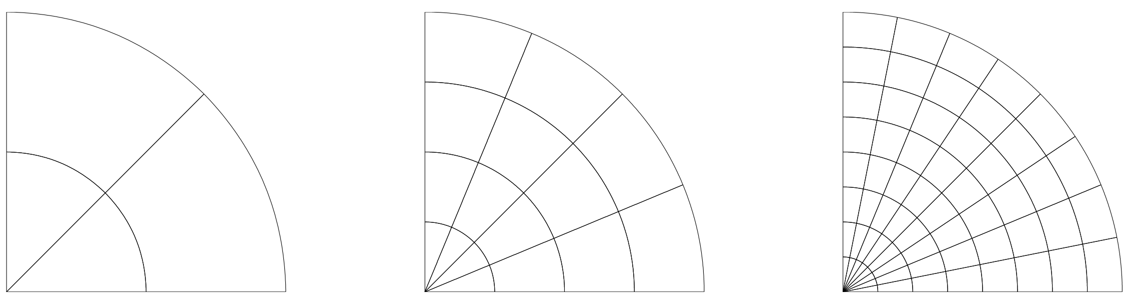

(a) $n_{el} = 2$ (b) $n_{el} = 4$ (c) $n_{el} = 8$

Figure 15: PM meshes with bi-quadratic mapping for circular plate problem

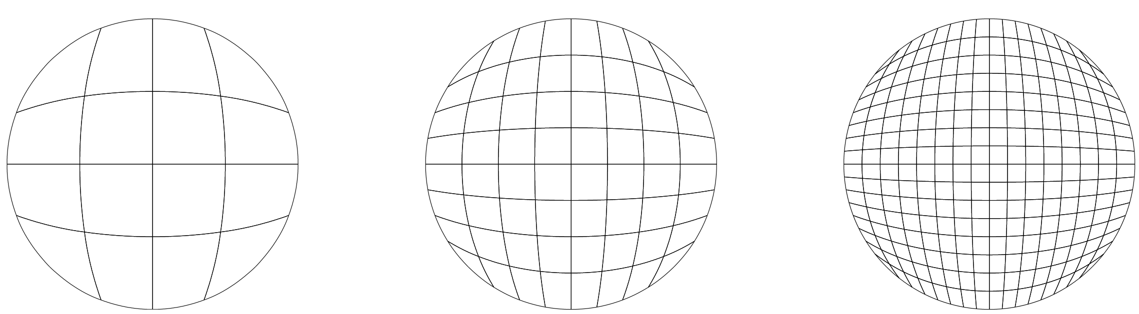

(a) $n_{el} = 2$ (b) $n_{el} = 4$ (c) $n_{el} = 8$

Figure 16: SCM meshes with bi-quadratic mapping for circular plate problem

	$t/L = 0.01$		$t/L = 0.001$		$t/L = 0.0001$	
Mesh	M_{max}	M_{min}	M_{max}	M_{min}	M_{max}	M_{min}
2×2	2.00063	1.27113	2.00090	1.27079	2.00090	1.27079
4×4	1.88260	1.40727	1.88092	1.41116	1.88090	1.41119
8×8	1.88789	1.28405	1.87024	1.32483	1.87001	1.32534
16×16	1.92966	1.13306	1.88602	1.24460	1.88357	1.25070
32×32	1.93351	1.12083	1.90501	1.15871	1.88817	1.20602
64×64	1.93390	1.12085	1.91713	1.10084	1.89412	1.16676
128×128	1.93400	1.12086	1.91731	1.10010	1.90766	1.10805

Table 14: Maximum and minimum principal "center" bending moments ($M \times 10^2/(qL^2)$) for second-order element simply-supported Morley's plate solutions for the three thickness/length ratios. Reference thin plate limit solutions evaluated retaining nine terms in the series are 1.9080 and 1.0834 [15].

4.3.1 Simply-Supported Case

We consider a simply-supported circular plate of radius $R = 1$, as illustrated in Figure 17.

For the PM-meshes, the only essential boundary condition imposed on the curved portion of the boundary is $w = 0$, while on the vertical and horizontal edges of the quadrant boundary the only essential boundary condition imposed is $\theta_n = 0$. For the SCM-meshes, the essential boundary condition imposed on the whole boundary is $w = 0$.

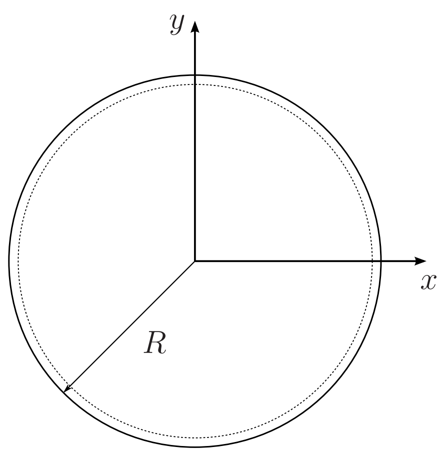

$E = 10^7$
$\nu = 0.3$
$k = 5/6$
$R = 1$
$t = 0.01, 0.001, 0.0001$
$q = 1$

Figure 17: Simply-supported circular plate model

We are particularly interested in studying the convergence of the central deflection, central bending moment about the x-axis, and bending moment about the y-axis at point $(x, y) = (R, 0)$ of the boundary. The exact Poisson-Kirchhoff solutions for these

	$t/R = 0.01$		$t/R = 0.001$		$t/R = 0.0001$	
Mesh	PM	SCM	PM	SCM	PM	SCM
2×2	0.82936	0.81177	0.82923	0.81166	0.82923	0.81166
4×4	0.94349	0.95153	0.94337	0.95143	0.94337	0.95143
8×8	0.98339	0.98787	0.98327	0.98777	0.98327	0.98777
16×16	0.99542	0.99704	0.99531	0.99694	0.99531	0.99694
32×32	0.99882	0.99933	0.99871	0.99924	0.99871	0.99923
64×64	0.99976	0.99991	0.99965	0.99981	0.99966	0.99981

Table 15: Center displacement $(w \times 64(1+\nu)D/((5+\nu)qR^4))$ for first-order element simply-suported circular plate solutions for the three thickness/length ratios. Reference thin plate limit solution is 1.0 [17].

	$t/R = 0.01$		$t/R = 0.001$		$t/R = 0.0001$	
Mesh	PM	SCM	PM	SCM	PM	SCM
2×2	0.99441	0.99947	0.99423	0.99937	0.99422	0.99937
4×4	0.99982	1.00006	0.99967	0.99996	0.99967	0.99995
8×8	1.00010	1.00010	0.99998	1.00000	0.99998	1.00000
16×16	1.00011	1.00010	1.00000	1.00000	0.99999	1.00000
32×32	1.00011	1.00010	1.00000	1.00000	0.99992	1.00000
64×64	1.00011	1.00010	1.00000	1.00000	0.99992	1.00000

Table 16: Center displacement $(w \times 64(1+\nu)D/((5+\nu)qR^4))$ for second-order element simply-supported circular plate solutions with bi-quadratic mapping for the three thickness/length ratios. Reference thin plate limit solution is 1.0 [17].

quantities are given by [17]:

$$w(0,0) = \left(\frac{5+\nu}{1+\nu}\right)\frac{qR^4}{64D} \tag{24a}$$

$$M_x(0,0) = (3+\nu)\frac{qR^2}{16} \tag{24b}$$

$$M_y(R,0) = (1-\nu)\frac{qR^2}{8} \tag{24c}$$

The convergence of the normalized center deflection obtained with the first- and second-order elements is displayed in Tables 15 and 16, respectively. Normalization is taken with respect to the exact Poisson-Kirchhoff solution (24a).

We next study the convergence of the normalized center bending moment about the x-axis. We sample the discrete bending moment at a quadrature point lying closest to the center of the plate. Tables 17 and 18 display the convergence of the center bending

	$t/R = 0.01$		$t/R = 0.001$		$t/R = 0.0001$	
Mesh	PM	SCM	PM	SCM	PM	SCM
2×2	0.41008	0.75691	0.41008	0.75690	0.41008	0.75690
4×4	0.34687	0.93594	0.34687	0.93594	0.34687	0.93594
8×8	0.32177	0.98378	0.32177	0.98378	0.32177	0.98378
16×16	0.31372	0.99593	0.31372	0.99593	0.31372	0.99593
32×32	0.31129	0.99898	0.31129	0.99898	0.31129	0.99898
64×64	0.31058	0.99974	0.31058	0.99975	0.31058	0.99974

Table 17: "Center" bending moment about the x-axis ($M_x \times 16/(qR^2(3+\nu))$) for first-order element simply-supported plate solutions for the three thickness/length ratios. Reference thin plate limit solution is 1.0 [17].

moment obtained using the two refinement schemes for the first- and second-order plate elements, respectively. The displayed center moments are scaled by the exact Poisson-Kirchhoff solution, given in this case by (24b). We note that the bending moment converges rapidly for the second-order discretization. However, for the polar mesh case, the first-order element bending moments do not converge to the true solutions. This may be attributed to the anticipated difficulties previously alluded to. To verify that this is a problem attributed to the lowest-order Raviart-Thomas vector fields, we solved the simply-supported circular plate problem with the standard selectively integrated bilinear Reissner-Mindlin element and found that the moments did in fact converge. This issue also occurs for the fully-clamped case; see the next section.

To conclude the analysis of the present example, we study the convergence of the bending moment about the y-axis at point $(x, y) = (R, 0)$ of the boundary. Tables 19 and 20 display the convergence of the bending moment obtained using the two refinement schemes for the first- and second-order plate elements, respectively. The displayed moments are scaled by (24c). Examining Table 19, we observe that, unlike the central bending moments obtained with the polar discretization scheme, no convergence issues seem to occur for the bending moment about the y-axis at point $(x, y) = (R, 0)$ of the boundary.

4.3.2 Fully-Clamped Case

Let us now consider the fully-clamped circular plate illustrated in Figure 18.

For the PM-meshes, essential boundary conditions $w = \theta_n = 0$ are imposed on the curved portion of the boundary, while on the vertical and horizontal edges of the quadrant boundary the only essential boundary conditions imposed are $\theta_n = 0$. For the SCM-meshes, essential boundary conditions $w = \theta_n = 0$ are imposed on the whole boundary.

We are interested in this case in the convergence of the central deflection, central bending moment about the x-axis, and bending moment about the x-axis at point $(x, y) = (R, 0)$ of the clamped edge. The exact Poisson-Kirchhoff solutions for these quantities

	$t/R = 0.01$		$t/R = 0.001$		$t/R = 0.0001$	
Mesh	PM	SCM	PM	SCM	PM	SCM
2×2	0.88524	0.98033	0.88251	0.98033	0.88247	0.98033
4×4	0.97411	0.99547	0.97026	0.99547	0.97011	0.99547
8×8	0.99379	0.99889	0.99296	0.99889	0.99250	0.99889
16×16	0.99845	0.99972	0.99843	0.99972	0.99814	0.99972
32×32	0.99961	0.99993	0.99961	0.99993	0.99938	0.99993
64×64	0.99990	0.99998	0.99990	0.99998	0.99970	0.99998

Table 18: "Center" bending moment about the x-axis ($M_x \times 16/(qR^2(3+\nu))$) for second-order element simply-supported plate solutions with bi-quadratic mapping for the three thickness/length ratios. Reference thin plate limit solution is 1.0 [17].

	$t/R = 0.01$		$t/R = 0.001$		$t/R = 0.0001$	
Mesh	PM	SCM	PM	SCM	PM	SCM
2×2	1.20381	1.32128	1.20381	1.32136	1.20381	1.32136
4×4	1.19732	1.27713	1.19732	1.27727	1.19732	1.27727
8×8	1.13215	1.15872	1.13215	1.15890	1.13215	1.15890
16×16	1.07526	1.08262	1.07526	1.08282	1.07526	1.08282
32×32	1.04000	1.04179	1.04000	1.04200	1.04000	1.04200
64×64	1.02060	1.02090	1.02060	1.02111	1.02061	1.02112

Table 19: Bending moment about the y-axis at point $(x, y) = (R, 0)$ of the boundary ($M_y \times 8/(qR^2(1-\nu))$) for first-order element simply-supported plate solutions for the three thickness/length ratios. Reference thin plate limit solution is 1.0 [17].

	$t/R = 0.01$		$t/R = 0.001$		$t/R = 0.0001$	
Mesh	PM	SCM	PM	SCM	PM	SCM
2×2	1.22662	1.28616	1.22619	1.28631	1.22618	1.28631
4×4	1.13080	1.14230	1.13062	1.14247	1.13061	1.14247
8×8	1.06880	1.07086	1.06879	1.07106	1.06878	1.07106
16×16	1.03516	1.03540	1.03515	1.03561	1.03515	1.03562
32×32	1.01775	1.01763	1.01775	1.01785	1.01769	1.01786
64×64	1.00892	1.00872	1.00892	1.00894	1.00886	1.00894

Table 20: Bending moment about the y-axis at point $(x, y) = (R, 0)$ of the boundary ($M_y \times 8/(qR^2(1-\nu))$) for second-order element simply-supported plate solutions with bi-quadratic mapping for the three thickness/length ratios. Reference thin plate limit solution is 1.0 [17].

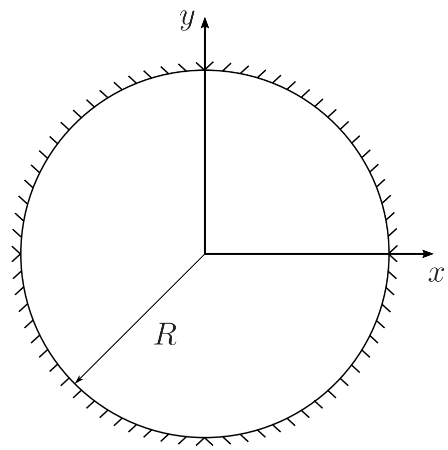

$E = 10^7$

$\nu = 0.3$

$k = 5/6$

$R = 1$

$t = 0.01, 0.001, 0.0001$

$q = 1$

Figure 18: Fully-Clamped circular plate model

	$t/R = 0.01$		$t/R = 0.001$		$t/R = 0.0001$	
Mesh	PM	SCM	PM	SCM	PM	SCM
2×2	0.84116	0.64189	0.84064	0.64117	0.84064	0.64116
4×4	0.94176	0.92727	0.94128	0.92682	0.94127	0.92682
8×8	0.98123	0.98313	0.98077	0.98272	0.98076	0.98272
16×16	0.99478	0.99615	0.99432	0.99575	0.99432	0.99574
32×32	0.99884	0.99935	0.99839	0.99894	0.99839	0.99894
64×64	1.00001	1.00014	0.99956	0.99974	0.99955	0.99973

Table 21: Center displacement ($w \times 64D/(qR^4)$) for first-order element fully-clamped circular plate solutions for the three thickness/length ratios. Reference thin plate limit solution is 1.0 [17].

are given by [17]:

$$w(0,0) = \frac{qR^4}{64D} \tag{25a}$$

$$M_x(0,0) = (1+\nu)\frac{qR^2}{16} \tag{25b}$$

$$M_x(R,0) = -\frac{qR^2}{8} \tag{25c}$$

Normalizations are taken with respect to these quantities.

We first study the convergence of the center displacement. Tables 21 and 22 display the convergence of the normalized center displacement for the first- and second-order plate elements, respectively, obtained for the two refinement schemes with various meshes.

We next study the convergence of the normalized bending moment about the x-axis at point $(x, y) = (R, 0)$ of the clamped edge. We sample the discrete bending moment at a

	$t/R = 0.01$		$t/R = 0.001$		$t/R = 0.0001$	
Mesh	PM	SCM	PM	SCM	PM	SCM
2×2	0.98752	1.00406	0.98707	1.00366	0.98706	1.00365
4×4	0.99984	1.00066	0.99939	1.00027	0.99938	1.00027
8×8	1.00043	1.00042	0.99998	1.00002	0.99997	1.00002
16×16	1.00046	1.00040	1.00000	1.00001	0.99999	1.00000
32×32	1.00046	1.00040	1.00000	1.00000	0.99997	1.00000
64×64	1.00046	1.00040	1.00000	1.00000	0.99995	1.00000

Table 22: Center displacement ($w \times 64D/(qR^4)$) for second-order element fully-clamped circular plate solutions with bi-quadratic mapping for the three thickness/length ratios. Reference thin plate limit solution is 1.0 [17].

	$t/R = 0.01$		$t/R = 0.001$		$t/R = 0.0001$	
Mesh	PM	SCM	PM	SCM	PM	SCM
2×2	0.26160	0.22495	0.26160	0.22478	0.26160	0.22478
4×4	0.59785	0.56414	0.59785	0.56398	0.59785	0.56397
8×8	0.79476	0.78106	0.79476	0.78088	0.79476	0.78088
16×16	0.89692	0.89274	0.89692	0.89255	0.89692	0.89255
32×32	0.94842	0.94741	0.94842	0.94720	0.94842	0.94720
64×64	0.97421	0.97410	0.97421	0.97389	0.97421	0.97389

Table 23: Bending moment about the x-axis at point $(x, y) = (R, 0)$ of the clamped edge ($M_x \times (-8)/(qR^2)$) for first-order element fully-clamped plate solutions for the three thickness/length ratios. Reference thin plate limit solution is 1.0 [17].

quadrature point lying closest to $(x, y) = (R, 0)$. Tables 23 and 24 display the convergence of the normalized bending moment obtained using the two refinement schemes for the first- and second-order plate elements, respectively. We note that the bending moment is converging linearly for both the first- and second-order cases, with the second-order case being the more accurate in absolute value.

We also study the convergence of the central bending moment about the x- axis. The obtained moments are presented in Tables 25 and 26, for the first- and second-order cases, respectively. We observe that, as in the simply-supported circular plate case with the polar discretization scheme, the first-order approximate solutions do not converge to the true solutions.

Finally, we study the convergence of the bending moment about the direction forming 45° with the x-axis at point $(x, y) = (R\cos(\pi/4), -R\sin(\pi/4))$ of the clamped edge obtained. We only use the SCM discretization scheme in this case. We note that point $(x, y) = (R\cos(\pi/4), -R\sin(\pi/4))$ is a singular point of the SCM meshes. The obtained

	$t/R = 0.01$		$t/R = 0.001$		$t/R = 0.0001$	
Mesh	PM	SCM	PM	SCM	PM	SCM
2×2	0.65090	0.64522	0.65090	0.64509	0.65090	0.64509
4×4	0.82572	0.82675	0.82572	0.82660	0.82572	0.82659
8×8	0.91282	0.91369	0.91282	0.91352	0.91282	0.91351
16×16	0.95641	0.95681	0.95641	0.95663	0.95641	0.95663
32×32	0.97820	0.97846	0.97820	0.97827	0.97819	0.97826
64×64	0.98910	0.98931	0.98910	0.98912	0.98908	0.98912

Table 24: Bending moment about the x-axis at point $(x, y) = (R, 0)$ of the clamped edge $(M_x \times (-8)/(qR^2))$ for second-order element fully-clamped plate solutions with bi-quadratic mapping for the three thickness/length ratios. Reference thin plate limit solution is 1.0 [17].

	$t/R = 0.01$		$t/R = 0.001$		$t/R = 0.0001$	
Mesh	PM	SCM	PM	SCM	PM	SCM
2×2	0.45741	0.55125	0.45741	0.55101	0.45741	0.55101
4×4	0.37522	0.89514	0.37522	0.89510	0.37522	0.89510
8×8	0.33227	0.97446	0.33227	0.97446	0.33227	0.97446
16×16	0.31720	0.99366	0.31720	0.99366	0.31720	0.99366
32×32	0.31237	0.99842	0.31237	0.99842	0.31237	0.99842
64×64	0.31090	0.99960	0.31090	0.99960	0.31090	0.99960

Table 25: "Center" bending moment about the x-axis $(M_x \times (16)/(qR^2(1 + \nu)))$ for first-order element fully-clamped plate solutions for the three thickness/length ratios. Reference thin plate limit solution is 1.0 [17].

	$t/R = 0.01$		$t/R = 0.001$		$t/R = 0.0001$	
Mesh	PM	SCM	PM	SCM	PM	SCM
2×2	0.75681	0.95270	0.75682	0.95270	0.75682	0.95270
4×4	0.93747	0.98871	0.93747	0.98871	0.93747	0.98871
8×8	0.98426	0.99720	0.98426	0.99720	0.98426	0.99720
16×16	0.99606	0.99930	0.99606	0.99930	0.99605	0.99930
32×32	0.99901	0.99982	0.99901	0.99983	0.99892	0.99983
64×64	0.99975	0.99995	0.99975	0.99996	0.99960	0.99996

Table 26: "Center" bending moment about the x-axis $(M_x \times (16)/(qR^2(1 + \nu)))$ for second-order element fully-clamped plate solutions with bi-quadratic mapping for the three thickness/length ratios. Reference thin plate limit solution is 1.0 [17].

Mesh	$t/L = 0.01$	$t/L = 0.001$	$t/L = 0.0001$
2×2	0.65992	0.66015	0.66015
4×4	0.91912	0.91945	0.91945
8×8	0.97554	0.97590	0.97591
16×16	0.99264	0.99308	0.99309
32×32	0.99798	0.99814	0.99814
64×64	1.00015	0.99954	0.99952

Table 27: Bending moment about the direction oriented 45° with respect to the x-axis at point $(x, y) = (R\cos(\pi/4), -R\sin(\pi/4))$ of the clamped edge $(M_x \times (-8)/(qR^2))$ for first-order element fully-clamped plate solutions with SCM meshes for the three thickness/length ratios. Reference thin plate limit solution is 1.0 [17].

Mesh	$t/L = 0.01$	$t/L = 0.001$	$t/L = 0.0001$
2×2	0.95362	0.95391	0.95391
4×4	0.97798	0.97837	0.97838
8×8	0.99430	0.99458	0.99458
16×16	1.00004	0.99875	0.99873
32×32	1.00163	0.99982	0.99970
64×64	1.00180	1.00023	0.99993

Table 28: Bending moment about the direction oriented 45° with respect to the x-axis at point $(x, y) = (R\cos(\pi/4), -R\sin(\pi/4))$ of the clamped edge $(M_x \times (-8)/(qR^2))$ for second-order element fully-clamped plate solutions with SCM meshes and bi-quadratic mapping for the three thickness/length ratios. Reference thin plate limit solution is 1.0 [17].

moments are displayed in Tables 27 and 28, for the first- and second-order cases, respectively. As it can be seen, the solutions are very accurate for both the first- and second-order cases.

5 Conclusions

We have generalized the twist-Kirchhoff formulation of rectangular plate elements to arbitrary quadrilateral elements. The key aspect of this generalization is the use of Piola transformed Raviart-Thomas rotation fields. This ensures that the normal components of rotation are continuous across element edges.

We have implemented the first two members of the twist-Kirchhoff family of elements and studied convergence and accuracy for non-rectangular element discretizations. Problems studied included linearly elastic square and circular simply-supported and clamped plates, and a simply-supported rhombic plate problem solved analytically by Morley [15].

In the square and rhombic plate problems we employed asymptotically parallelogram-shape-regular meshes, and satisfactory convergence of all quantities considered was realized.

In the case of circular plates, we studied polar meshes, in which the quadrilateral elements are degenerated to triangles at the center of the plate creating a singularity in the geometric mapping, and meshes in which a square is mapped to a circle, for which there are four singular points in the geometrical mapping on the boundary of the plate. We were particularly curious about the behavior of the bending moments at the singular points. For the second-order element, all quantities, including the bending moments at the singularities, converged nicely for all meshes. For the first-order elements, all quantities converged nicely except for the bending moments at the singularity at the center of the plate where the quadrilateral elements were degenerated into triangles. We argued on theoretical grounds why the first-order element cannot be degenerated into a triangle and our numerical results for the polar meshes support this conclusion. A convergent triangular element with exactly the same vertex displacement and mid-edge normal rotation degrees-of-freedom is the famous Morley triangle [16], which can be recommended as an alternative to degenerating the lowest-order twist-Kirchhoff quadrilateral.

Aside from this one admonition to avoid degenerating the lowest-order elements to triangles, we find the overall accuracy of the elements satisfactory for considering their use for solving practical plate problems. The main attribute of these elements is their unique combination of efficiency and robustness, that is, they require only $r \times r$ Gauss quadrature, where r is the order of the elements, to produce stable elements with no hourglass or other singular modes. We believe this attribute is an important and potentially deciding one in explicit dynamic analysis for which solution times and storage requirements scale with the number of quadrature points.

Acknowledgements

H.A.F.A. Santos was supported by the Fundação para a Ciência e a Tecnologia of Portugal under the Post-Doc Grant No. SFRH/BPD/33950/2009. J.A. Evans was partially supported by the Department of Energy Computational Science Graduate Fellowship, provided under grant number DE-FG02-97ER25308. T.J.R. Hughes was partially supported by the Office of Naval Research under Contract No. N00014-08-0992 and by the National Science Foundation under Grant No. 0700204. This support is gratefully acknowledged.

References

[1] D N Arnold, D Boffi, and R S Falk. Quadrilateral $H(\mathrm{div})$ finite elements. *SIAM Journal on Numerical Analysis*, 42:2429–2451, 2004.

[2] K J Bathe and E Dvorkin. A 4-node plate bending element based on Mindlin-Reissner theory and a mixed interpolation. *International Journal for Numerical Methods in Engineering*, 21:367–383, 1985.

[3] T Belytschko and W Bachrach. Efficient implementation of quadrilaterals with high coarse-mesh accuracy. *Computer Methods in Applied Mechanics and Engineering*, 54:279–301, 1986.

[4] T Belytschko and C S Tsay. A stabilization procedure for the quadrilateral plate element with one-point quadrature. *International Journal for Numerical Methods in Engineering*, 19:405–419, 1983.

[5] A Bermudez, P Gamallo, M R Noguerias, and R Rodriguez. Approximation properties of lowest-order hexahedral Raviart-Thomas finite elements. *Comptes Rendus Mathematique*, 340:687–692, 2005.

[6] K Bletzinger, M Bischoff, and E Ramm. A unified approach for shear-locking-free triangular and rectangular shell finite elements. *Computers and Structures*, 75:321–334, 2000.

[7] F Brezzi, K J Bathe, and M Fortin. Mixed-interpolated elements for Reissner-Mindlin plates. *International Journal for Numerical Methods in Engineering*, 28:1787–1801, 1989.

[8] F Brezzi, J A Evans, T J R Hughes, and L D Marini. New rectangular plate elements based on twist-Kirchhoff theory. *Computer Methods in Applied Mechanics and Engineering*, 200:2547–2561, 2011.

[9] F Gruttmann and W Wagner. A stabilized one-point integrated quadrilateral Reissner-Mindlin plate element. *International Journal for Numerical Methods in Engineering*, 61:2273–2295, 2004.

[10] T J R Hughes. *The Finite Element Method: Linear Static and Dynamic Finite Element Analysis*. Dover Publications, Inc., New York, 2000.

[11] T J R Hughes, M Cohen, and M Haroun. Reduced and selective integration techniques in finite element analysis of plates. *Nuclear Engineering and Design*, 46:203–222, 1978.

[12] T J R Hughes, R L Taylor, and W Kanoknukulchai. Simple and efficient finite element for plate bending. *International Journal for Numerical Methods in Engineering*, 11:1529–1543, 1977.

[13] T J R Hughes and T E Tezduyar. Finite elements based upon Mindlin plate theory, with particular reference to the 4-node bilinear isoparametric element. *Journal of Applied Mechanics*, 48:587–595, 1981.

[14] R H MacNeal. Derivation of element stiffness matrices by assumed strain distribution. *Nuclear Engineering & Design*, 70:3–12, 1982.

[15] L S D Morley. *Skew Plates and Structures*. Pergamon Press, Oxford, 1963.

[16] L S D Morley. The constant-moment plate-bending element. *Journal of Strain Analysis*, 6:20–24, 1971.

[17] J N Reddy. *Theory and Analysis of Elastic Plates and Shells*. CRC Press, Taylor & Francis Group, Boca Raton, 2007.

[18] M Rossow. Efficient C^0 finite-element solution of simply supported plates of polygonal shape. *Journal of Applied Mechanics, ASME*, 44:347–349, 1977.

[19] R L Taylor and S Govindjee. Solution of clamped rectangular plate problems. *Communications in Numerical Methods in Engineering*, 20:757–765, 2004.

[20] S Timoshenko and S Woinowsky-Krieger. *Theory of Plates and Shells*. McGraw-Hill Book Company, Inc., New York, 1959.